Available online at www.sciencedirect.com
SCIENCE DIRECT®
Physics of the Earth and Planetary Interiors 152 (2005) 191–199
PHYSICS OF THE EARTH AND PLANETARY INTERIORS
www.elsevier.com/locate/pepi

Texture development and deformation mechanisms in ringwoodite

H.-R. Wenk [a,b,*], G. Ischia [a,c], N. Nishiyama [d], Y. Wang [d], T. Uchida [d]

[a] *Department of Earth and Planetary Science, University of California, Berkeley, CA 94720, USA*
[b] *GeoForschungsZentrum Potsdam, 14473 Potsdam, Germany*
[c] *Dip. Ingegneria dei Materiali e Tecnologie Industriali, Università Trento, 38050 Trento, Italy*
[d] *Center for Advanced Radiation Sources, The University of Chicago, 5640 South Ellis Avenue, Chicago, IL 60637, USA*

Received 20 December 2004; received in revised form 28 May 2005; accepted 16 June 2005

Abstract

Ringwoodite Mg_2SiO_4 with spinel structure is an important phase in the earth's mantle transition zone. Controlled deformation experiments showed that ringwoodite underwent ductile deformation when compressed axially at 6–10 GPa and at room temperature in a multianvil D-DIA deformation apparatus. Texture evolution during cyclic compression has been recorded in situ using X-ray transparent anvils with monochromatic synchrotron X-ray diffraction and a two-dimensional detector. Quantitative analysis of the images with the Rietveld method revealed a 1 1 0 fiber texture. By comparing this texture pattern with polycrystal plasticity simulations, it is inferred that $\{1\,1\,1\}\langle\bar{1}\,1\,0\rangle$ slip is the dominant deformation mechanism in ringwoodite, consistent with high temperature mechanisms observed in other spinel-structured materials. Although strong ringwoodite textures may develop in the transition zone, the contribution to bulk anisotropy is minimal due to the weak single-crystal anisotropy.

Keywords: Ringwoodite; Texture; Multianvil apparatus; Synchrotron X-rays; Deformation mechanisms; Transition zone

1. Introduction

In the transition zone, at depths between 500 and 700 km, olivine, the major phase in the earth's upper mantle, transforms to wadsleyite and ringwoodite, which, in turn, transform to perovskite and ferropericlase in the lower mantle. Ringwoodite is thought to be a major phase in subducting slabs at depths from 520 to 670 km (Irifune and Ringwood, 1987). Geodynamicists are debating whether this layer, composed largely of minerals with garnet, ilmenite and spinel-type structures, acts as a separation between convection cells or if subducting and upwelling slabs cross it without much interaction (King, 1995; Panasyuk and Hager, 1998). Seismologists have established in tomographic maps considerable heterogeneity and anisotropy (Trampert

* Corresponding author. Tel.: +1 510 642 7431; fax: +1 510 643 9980.
E-mail address: wenk@seismo.berkeley.edu (H.-R. Wenk).

0031-9201/$ – see front matter © 2005 Elsevier B.V. All rights reserved.
doi:10.1016/j.pepi.2005.06.008

and Van der Heijst, 2002; Wookey et al., 2002), to which preferred orientation of ringwoodite may contribute.

Thus, mineral physicists have become interested in elastic and plastic properties of minerals, such as majorite (Jin et al., 2001; Karato et al., 1995), wadsleyite (Thurel et al., 2003; Yamazaki and Karato, 2001a) and ringwoodite (e.g. Chen et al., 2001; Karato et al., 1998; Kavner and Duffy, 2001) making use of new experimental possibilities, especially the rotational Drickamer apparatus (Yamazaki and Karato, 2001b) and the D-DIA multianvil apparatus (Wang et al., 2003). In this report, we present a first application of in situ texture measurements with the D-DIA by investigating texture development of ringwoodite during triaxial deformation. Diffraction images are analyzed with the Rietveld method and intensity variations along Debye rings are used to derive the orientation distribution function (ODF) with an approach similar to that used for radial diamond anvil cell experiments (Wenk et al., 2004). The observed texture patterns are then compared with polycrystal plasticity simulations to obtain information about slip systems operating in ringwoodite. Conclusions from these room temperature experiments cannot be directly applied to mantle conditions but they provide a basis for extrapolation to other conditions. Results can be compared with other compounds of spinel structure and are thus useful in establishing the rheology of ringwoodite and implications for anisotropy in the transition zone.

2. Experimental techniques

The deformation experiment was performed at beamline 13-BM-D of the Advanced Photon Source, at station GSECARS, with monochromatic X-rays (wavelength 0.191 Å), a two-dimensional (2D) X-ray detector and a radiographic imaging system. Details of the D-DIA and experimental procedures are described elsewhere (Wang et al., 2003; Uchida et al., 2004). Fig. 1 is a sketch of the experimental facility. The sample was a pre-sintered, fully densified polycrystalline stoichiometric Mg_2SiO_4 ringwoodite aggregate, of grain size 10 μm, synthesized at 20 GPa and 1523 K at the Geodynamics Research Center, Ehime University.

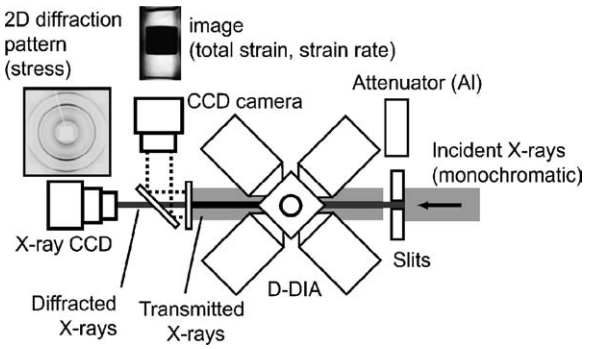

Fig. 1. Sketch of the experimental setup with D-DIA deformation apparatus, synchrotron X-ray beam, X-ray CCD (SMART-1500) to record the diffraction pattern and an imaging CCD camera for sample length measurement. Note that certain diffracted X-rays must pass through portions of the cBN anvils, resulting in an intensity contrast that needs to be corrected for quantitative textural analysis.

We used four sintered cubic boron nitride (cBN) anvils with truncated edge lengths of 3 mm. These X-ray transparent anvils permitted observation of diffraction Debye rings over the entire 360° azimuthal range. Incident X-rays were collimated to 100 μm × 100 μm by two pairs of tungsten carbide (WC) slits and directed to the sample through the anvil gap and pressure media. The 2D diffraction patterns were collected with a CCD detector (SMART-1500) mounted perpendicular to the incident X-ray. The precise detector orientation relative to the incident beam was calibrated with a diffraction standard (CeO_2) and the detector–sample distance by matching the observed ambient *d*-values of the sample inside the D-DIA to those reported by Sasaki et al. (1982). Throughout the experiment, the sample length was measured by radiography, using a wide X-ray beam (3 mm × 3 mm cross section), by driving the WC slits out of the beam path. The cell assembly was similar to that used in Uchida et al. (2004). The 5 mm edge length cubic pressure medium was made of amorphous boron powder and epoxy. The sample (0.8 mm in diameter and 1.2 mm in length, with both ends carefully polished to be parallel) was inserted in a 1.6 mm diameter chamber in the cube, lined with a hexagonal boron nitride sleeve. Two alumina pistons, with both ends also polished, were placed just above and below the sample, with gold foils in between, serving as strain markers. From Fig. 1, it is clear that diffracted X-rays pass through various components of the D-DIA apparatus and are partially

absorbed. The direction-dependent absorption has to be accounted for in data processing.

The sample was first compressed quasi-hydrostatically to a ram load of 30 t, during which process the sample was shortened by about 20%. Subsequently, nine shortening and lengthening deformation cycles were carried out by advancing and retracting the differential ram pistons at various speeds, first at 30 t (∼4–7 GPa), then at 50 t (∼7–10 GPa). Pressure was determined based on the third-order Birch-Murnaghan equation of state for ringwoodite (Meng et al., 1994), using the *d*-spacings measured at the "magic" azimuth angle, where the effect of differential stress on pressure is zero (Singh, 1993). In each deformation cycle, an average strain rate was calculated based on sample length measurements during deformation, beyond the yield point. Strain rates ranged from $\sim 4.7 \times 10^{-6}$ to $\sim 5.8 \times 10^{-5}\ s^{-1}$. Values of differential stress were calculated based on the lattice strain determination, using single-crystal elasticity data (Weidner et al., 1984) and pressure derivatives (Sinogeikin and Bass, 2001) for ringwoodite. The maximum differential stress was about 5 GPa. The maximum total axial compressive strain reached was 45% (where strain is defined as $(l_0 - l)/l_0$, with l_0 being the sample length after hydrostatic compression). Cycling occurred between 20 and 45% shortening. After cyclic compression, the sample was recovered and, at ambient conditions, it displayed a permanent axial shortening strain of 37%. Details of the mechanical data and their analysis have been reported in a separate paper (Nishiyama et al., 2005).

In this study, we analyzed five images, selected out of the 2D patterns (275) collected. The first one is immediately after hydrostatic compression, before the deformation cycles. Three images were selected at different strains during the first deformation cycle. All of these were recorded in situ in the D-DIA apparatus at pressure. The last image was obtained at ambient conditions after the sample was removed from the apparatus. Fig. 2 shows two diffraction images recorded. The compression direction is vertical (arrows). The innermost diffraction ring is 0 0 0 2 from the highly compressible boron nitride sleeve, all others are from ringwoodite. The first image is from the specimen that was removed from the apparatus after multiple deformation cycles (Fig. 2a). There are strong intensity variations along Debye rings that are different for different diffraction peaks; 2 2 0 is marked as an example with intensity maxima parallel to the compression direction. These variations are due to crystallite preferred orientation (texture) and are of primary interest in this study. The second image (Fig. 2b) is recorded in situ in the D-DIA apparatus during hydrostatic compression and loading to 27%. Intensities are lower (brighter) on the left and right sides of the image than in the central section, affecting both diffraction peaks and background. This azimuthal intensity variation is due to anvil absorption and shadowing of diffracted X-rays, as well as background scattering by the apparatus (Fig. 1). In addition, there is an intensity variation along Debye rings that is due to texture as in Fig. 2a. Intensity variations in the in situ images that are due to anvil absorption will have to be removed by data processing to reveal the true textures.

3. Data analysis

For the analysis of the diffraction images, we relied on the Rietveld method as implemented in MAUD (Lutterotti et al., 1999). Synchrotron diffraction images can be directly analyzed for structural parameters, microstructure, stress state and texture, and the method has been developed and tested for biomineralogical textures with complex diffraction patterns (Lonardelli et al., 2005) and applied to diamond anvil deformation experiments (Wenk et al., 2004). First, the image center is determined manually and a region of interest is established. For the deformed samples, the images were divided into 72 angular 5° slices and integrated to produce spectra, such as those shown in Fig. 3 at different azimuthal angles ((→) is parallel to compression and (←) perpendicular to compression). Peak intensity variations are indicative of texture. The 4 4 0 diffraction peak, for example, has a much higher intensity parallel to the shortening direction than perpendicular to it. The image before loading (D0493_001) has been divided into 24 slices and integrated over 15° to improve statistics. The starting material is rather coarse grained, with a spotty diffraction pattern. During deformation, the effective grain size (region of coherent diffraction) decreases and Debye rings become smooth as in Fig. 2. The image analysis was complicated by the fact that the CCD camera has a different pixel size in the horizontal and vertical direction.

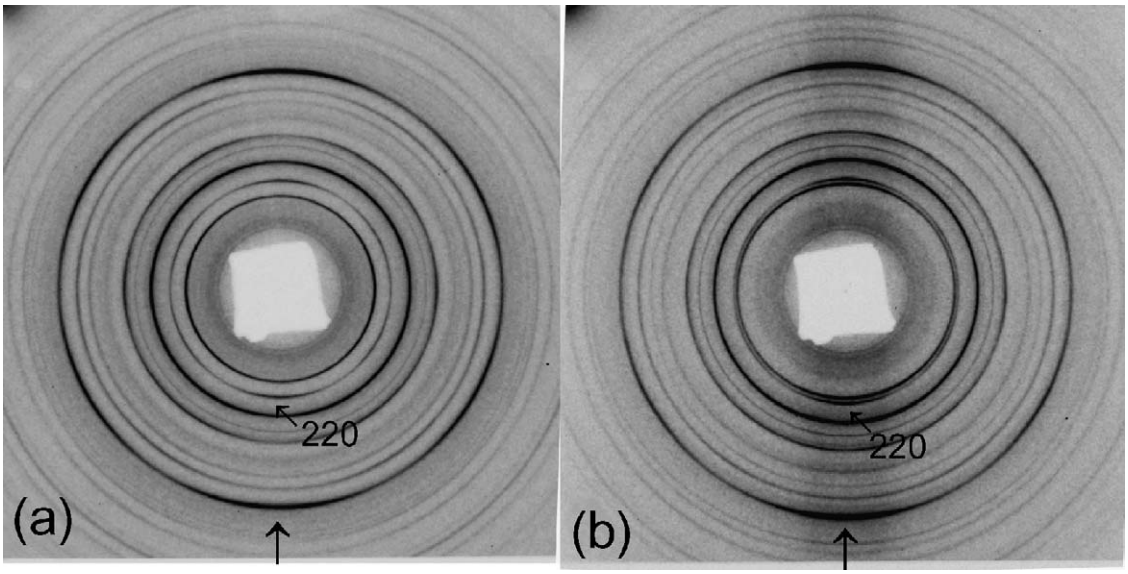

Fig. 2. CCD image recording diffraction pattern of ringwoodite: (a) sample after multicyclic axial deformation and recovered from the deformation apparatus (D0493_274) and (b) material during load, recorded in situ in the D-DIA apparatus (D0493_028). Vertical arrow indicates the compression direction.

The refinement considers instrumental parameters, such as image center, peak shape described by the Caglioti function, a scale factor for each spectrum and three background parameters. The scale factors are used to account for the azimuthal absorption variation. For each image, we then refined structural and microstructural parameters, as well as differential stress. The stress was refined only for the samples under axial load and is relative to the compressed sample before deformation.

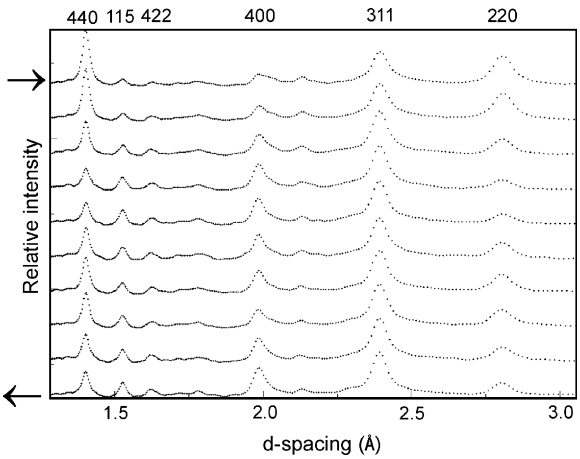

Fig. 3. Diffraction spectra integrated over a 5° angular range. Some peaks are indexed. Only 10 spectra, from parallel to perpendicular to the compression direction in 10° intervals are displayed (D0493_274). The arrow (→) is parallel to the compression direction and (←) perpendicular to it.

For the texture refinement, we used the EWIMV model that relies on the discrete tomographic method WIMV (Matthies and Vinel, 1982) but allows for arbitrary pole figure coverage. For projection tube radius, we chose 10°, and for ODF resolution 5°. The refined ODF was exported from MAUD and further smoothed in BEARTEX (Wenk et al., 1998) with a 7.5° Gauss filter to avoid artefacts from the cell structure. For the texture calculations, displayed in inverse pole figures (Fig. 4), an axial symmetry about the compression direction was imposed. The inverse pole figures represent the probability of finding crystal directions parallel to the shortening (axial) direction. Densities are expressed in multiples of a random distribution.

4. Results

The lattice parameter of ringwoodite was refined using the image of the sample before load application

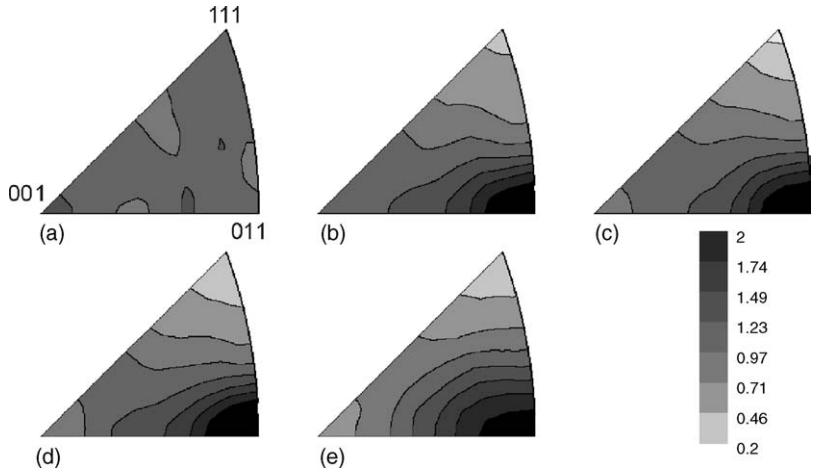

Fig. 4. Inverse pole figures for ringwoodite: (a) at 6 GPa confining pressure before axial compression (D0493_001); (b) in compression 22% strain (D0493_011); (c) in compression 25% strain (D0493_022); (d) in compression 27% strain (D0493_028); (e) recovered sample 37% strain (D0493_274). Equal area projection. Grey shades display pole densities in m.r.d. with linear scale contours.

but at hydrostatic pressure (D0493_001) (Table 1). For images with load, the lattice parameter was kept constant. This allows the evaluation of principal stresses (σ_{11}, σ_{22}, σ_{33}) with a simple triaxial stress model. Taking account the deformation geometry, only σ_{11} and σ_{33} were refined, and σ_{22} was kept equal to σ_{11} consistent with axial compression. Average pressure (4.8–7.5 GPa) as well as differential stress results (2.3–4.3 GPa at 22–27% shortening) determined with the triaxial stress model are compatible with those obtained independently (4–7 and <5 GPa, respectively, Nishiyama et al., 2005). The lattice parameter of the recovered sample at ambient conditions agrees with values in the literature (Sasaki et al., 1982; Utsumi et al., 1995).

Crystallite sizes and microstrain have also been refined and values are listed in Table 1 for each image. The crystallite size is large in the starting material (∼4 μm), consistent with values measured by microscopy of 5–10 μm), but the size decreases rapidly during deformation so that coherently scattering domains are around 0.1 μm.

Texture information is summarized in Fig. 4 and Table 1. The starting material shows no significant texture (Fig. 4a). All other samples display a moderate 1 1 0 fiber texture (Fig. 4b–e), implying that (1 1 0) lattice planes are preferentially aligned perpendicular to the compression direction. In the three images analyzed in situ under load, the texture does not change much and the texture strength (expressed by the texture index F_2, Bunge, 1982, which is the squared integral over the ODF) ranges between 1.17 and 1.22. This is not unexpected since shortening strains are similar (22–27%). The recovered sample has the strongest

Table 1
Structural and textural information for ringwoodite

	Before deformation	22% Strain	25% Strain	27% Strain	35% Recovered
Image	D0493_001	D0493_011	D0493_022	D0493_028	D0493_274
a (Å)	7.9034 (5)	7.9034	7.9034	7.9034	7.9371 (3)
Crystallite size (μm)	4 (5)	0.108 (7)	0.109 (3)	0.081 (3)	0.051 (1)
Microstrain	1E − 8	3.7E − 4	1.1E − 4	1.5E − 3	2.9E − 4
Average pressure (GPa)	∼6	4.8	6.9	7.5	
Differential stress (GPa)		2.3	3.0	4.3	
F_2 (m.r.d.)	1.01	1.17	1.19	1.22	1.24
ODF min–max (m.r.d.)	0.76–1.29	0.35–2.22	0.14–2.26	0.25–2.45	0.26–2.24

texture ($F_2 = 1.24$) consistent with the most extensive loading history and the largest shortening (37%) (Fig. 4e).

5. Discussion

The experimental texture data confirm mechanical results (Nishiyama et al., 2005) that ringwoodite deforms plastically at room temperature and 5–10 GPa confining pressure. This is consistent with diamond anvil cell experiments documenting that at high pressure, silicates and oxides such as olivine, perovskite and periclase deform ductily at low temperature (Merkel et al., 2002, 2003; Wenk et al., 2004). In the case of ringwoodite, in axial deformation and overall shortening geometry, a well-defined 1 1 0 fiber texture develops at strains between 22 and 37%. There is not much change in this pattern, even after several deformation cycles. From texture patterns, we can infer active deformation mechanisms by comparing experimental observations with results obtained from polycrystal plasticity models.

Polycrystal plasticity models, such as Taylor (upper bound) or Sachs (lower bound), assume intracrystalline deformation mechanisms like slip and mechanical twinning (Kocks, 2000). A deformation path is applied in increments to a set of initial orientations. During each increment, as crystals deform, grains are reoriented and rotated relative to the applied stress field. The rotations depend on the active slip systems and thus, from the final textural pattern, the slip systems can be inferred. A useful procedure is to model texture development for different slip systems and then determine which pattern best compares with experimental results. Polycrystal plasticity simulations were done with the viscoplastic self-consistent model that is closer to stress equilibrium than strain compatibility (Tomé and Canova, 2000), using the Los Alamos computer code VPSC (Lebensohn and Tomé, 1994). In our case, we assume 1000 random orientations, corresponding to the starting material with no texture (Fig. 4a).

Slip systems in spinel structures have been investigated in detail by ceramicists (see review by Mitchell, 1999). Slip on various planes has been documented, all with $\langle 1\,1\,0\rangle$ as slip direction (Table 2). Most of the studies have been made at high temperatures but in our experiments, ductility was achieved by high confining pressure. There is an early report of mechanical twinning in magnetite (Grün, 1918) but this has not been confirmed in more recent studies of spinel deformation. We investigated the activity of different systems by assigning different critical resolved shear stresses.

Table 2
Deformation mechanisms in spinel structures (Mitchell, 1999)

Slip system	A	B	C	D	E
$\{1\,1\,1\}\langle\bar{1}\,1\,0\rangle$	1 (100)	7 (0)	7 (1)	1 (58)	1 (6)
$\{1\,1\,0\}\langle\bar{1}\,1\,0\rangle$	7 (0)	1 (95)	7 (1)	1 (10)	1 (0)
$\{0\,0\,1\}\langle\bar{1}\,1\,0\rangle$	7 (0)	7 (5)	1 (98)	1 (31)	1 (8)
$\{1\,1\,1\}\langle\bar{2}\,1\,1\rangle$ Twinning	9 (0)	9 (0)	9 (0)	9 (0)	1 (86)

Relative critical resolved shear stress coefficients assumed in the polycrystal plasticity simulations shown in Fig. 5. Also shown are average slip system activities (in brackets in %) at 20% strain.

Calculations were done with different assumptions of critical resolved shear stresses (Models A–E in Table 2). In all cases, $n = 9$ was used as stress exponent to account for strain rate sensitivity. This was done in accordance with other simulations of low temperature experiments (Tomé and Canova, 2000) and has little influence on texture results. Ten strain increments of 2% were applied and the resulting texture patterns are evaluated in inverse pole figures of the shortening/lengthening direction (Fig. 5). The inverse pole figures are obtained by first entering individual orientations into a continuous ODF, filtering with a 10° Gauss function to smooth the cell structure and then calculating inverse pole figures from the ODF.

The results of the simulations show considerable diversity but also some similarities. The best agreement with experiments was observed when $\{1\,1\,1\}\langle\bar{1}\,1\,0\rangle$ slip is predominantly active (Models A and D, Fig. 5a and d). Only activating $\{1\,1\,0\}$ slip produces a weak texture with a maximum at (0 0 1) (Model B, Fig. 5b). This slip system is active in MgO at low temperature (Merkel et al., 2002) and, as has been explained by Wenk et al. (1989), the $\{1\,1\,0\}\langle\bar{1}\,1\,0\rangle$ slip system is special because for each system $(1\,1\,0)[1\,1\,0]$ there is an equivalent system $(1\,\bar{1}\,0)[1\,1\,0]$ (slip plane and slip direction exchanged) with exactly the same Schmidt factor and therefore the same activity, thus cancelling rotations. Texture evolution in this case is only due to the evolution of anisotropic grain shape during deformation and thus weak at low strains. For Model C, only $\{1\,0\,0\}$ slip is active. The texture (Fig. 5c) is not very

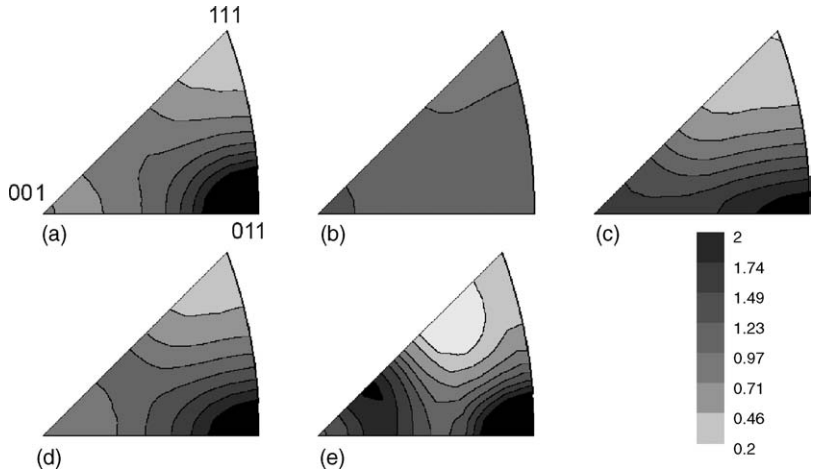

Fig. 5. Inverse pole figures obtained from polycrystal plasticity simulations for 20% shortening and assuming different activity of slip systems. (a), (b), etc. correspond to Models A, B, etc. in Table 2. Equal area projection. Grey shades display pole densities in m.r.d. with linear scale contours.

different from Model A (Fig. 5a), though there is a distinct shoulder towards (0 0 1) and texture evolution is weaker. If all slip systems have equal critical shear stress coefficients (Model D), $\{1\,1\,1\}$ is by far the most active system because of symmetry multiplicity and the texture resembles that of Model A (Fig. 5d versus Fig. 5a). Finally, if mechanical twinning is activated (Model E) the resulting simulated texture is very different from the one which is observed (Fig. 5e). Thus, the $\{1\,1\,1\}\langle\bar{1}\,1\,0\rangle$ slip system is mainly responsible for the main 1 1 0 concentration in the inverse pole figure. Significant mechanical twinning can be excluded, since it would produce textures that are inconsistent with the observations. We note that $\{1\,1\,1\}\langle\bar{1}\,1\,0\rangle$ slip is the main deformation system in fcc metals and in those also produces 1 1 0 fiber textures (Rollett and Wright, 2000).

These D-DIA deformation experiments were performed at room temperature. Naturally, for geophysical applications, slip systems and texture development at high temperature need to be known. So far such experiments at mantle conditions do not exist. But we point out that $\{1\,1\,1\}\langle\bar{1}\,1\,0\rangle$ is in fact the slip system that was observed in $MgAl_2O_4$ spinel at high temperature and ambient pressure (Mitchell, 1999) and it is likely that it is also the most active system at pressures and temperatures of the transition zone. As a general rule, with increasing temperature potential slip systems tend to have more similar critical shear stresses and systems that are harder at low temperature become activated. Examples are NaCl (Carter and Heard, 1970), MgO (Merkel et al., 2002; Stretton et al., 2001; Yamazaki and Karato, 2002) and calcite (De Bresser and Spiers, 1997). Thus, for high temperature high pressure deformation of ringwoodite, it is expected to have mechanisms close to those of Model D in Table 2. In the future, we plan to verify this with D-DIA experiments at high temperature. Also, molecular dynamics calculations may soon be able to extrapolate critical shear stresses to different pressure and temperature conditions (Miranda and Scandolo, 2005).

For high pressure deformation experiments, different apparatus are available, each with advantages and disadvantages. For ultrahigh pressures, corresponding to conditions of the deeper lower mantle and core, presently only the diamond anvil cell technique can be used (e.g. Merkel et al., 2002). This method is relatively simple and inexpensive. Disadvantages are small sample volumes (e.g. 80 μm × 80 μm × 30 μm), requiring small grain size and often poor grain statistics for textural studies. Also, deformation, stress, and confining pressure cannot be separated, stresses are very high and strain rates are difficult to quantify. The rotational Drickamer apparatus with a torsion geometry can be used for pressures of the transition zone and enables deformation in simple shear that is often of

interest to produce large strains (Yamazaki and Karato, 2001b). It can be applied to relatively large samples (>1 mm × 1 mm × 1 mm at 16 GPa and a temperature up to 2000 K). However, in torsion, strain is heterogeneous and so far, with this technique, textures cannot be measured in situ at pressure. The D-DIA multianvil apparatus is also limited to pressures of the transition zone but has the advantage that large samples (1–2 mm) can be deformed homogeneously in a variety of coaxial strain geometries. Stress and confining pressure are easily separated and mechanical data are accurately measured. Experiments can be conducted not only at pressure, but also at temperature (up to 1400 K) and in situ texture measurements can be performed, as this investigation demonstrates. We expect that the method described here will be extremely useful to study plasticity at pressure in a wide range of materials.

Having established that ringwoodite may develop strong textures if deformation is accommodated by dislocation glide, we have to evaluate how preferred orientation of this mineral could conceivably produce seismic anisotropy that has been revealed in the transition zone (Trampert and Van der Heijst, 2002; Wookey et al., 2002). Elastic anisotropy of the polycrystal is obtained by averaging single-crystal elastic properties over the orientation distribution. However, elastic anisotropy of ringwoodite at pressure and temperature of the transition zone is less than 3% (Karki et al., 2001). Averaging will reduce this value considerably, particularly because of cubic crystal symmetry, and thus it is unlikely that ringwoodite could contribute significantly to seismic anisotropy in the transition zone.

6. Conclusions

Deformation experiments with the D-DIA multianvil apparatus establish that ringwoodite deforms in a ductile fashion at room temperature and a confining pressure up to 10 GPa. In situ observations with synchrotron X-rays document strong texture evolution already at moderate strains of 20–30%. From the observed 1 1 0 fiber texture, it is concluded that dislocation glide on $\{1\,1\,1\}\langle\bar{1}\,1\,0\rangle$ is the primary slip system in ringwoodite consistent with slip systems in other spinel structures. Similar experiments with D-DIA can be used to investigate in situ plastic and elastic deformation at pressure and temperature.

Acknowledgements

We appreciate discussions with Terry Mitchell (LANL), Luca Lutterotti (Trento), Sebastien Merkel (Lille), Frank Schilling (Potsdam) and Sergio Speziale (Berkeley) as well as suggestions from reviewers. HRW is grateful for hospitality at GFZ Potsdam during a sabbatical leave. We acknowledge access to the facilities of APS and financial support from CDAC, IGPP and NSF. GeoSoilEnviroCARS is supported by the National Science Foundation, Earth Sciences (EAR-0217473), Department of Energy, Geosciences (DE-FG02-94ER14466) and the State of Illinois. Use of the APS was supported by the U.S. Department of Energy, Basic Energy Sciences, Office of Energy Research, under Contract No. W-31-109-Eng-38. N.N is partly supported by Postdoctoral Fellowships for Research Abroad of Japan Society for the Promotion of Science.

References

Bunge, H.-J., 1982. Texture Analysis in Materials Science—Mathematical Methods. Butterworths, London.

Carter, N.L., Heard, H.C., 1970. Temperature and rate-dependent deformation of halite. Am. J. Sci. 269, 193–249.

Chen, J., Inoue, T., Weidner, D.J., Wu, Y., Vaughan, M.T., 2001. Strength and water weakening of mantle minerals, olivine, wadsleyite and ringwoodite. Geophys. Res. Lett. 25, 575–578.

De Bresser, J.H.P., Spiers, C.J., 1997. Strength characteristics of the r, f and c slip systems in calcite. Tectonophysics 272, 1–23.

Grün, A., 1918. Künstliche Zwillingsbildung des Magnetit. N. Jb. Miner. Geol. und Paleont. (Jahrbuch), 99–112.

Irifune, T., Ringwood, A.E., 1987. Phase transformations in a harzburgite composition to 26 GPa: implications for dynamical behaviour of the subducting slab. Earth Planet. Sci. Lett. 86, 365–376.

Jin, Z.M., Zhang, J., Green, H.W., Jin, S., 2001. Eclogite rheology: implications for subducting lithosphere. Geology 29, 667–670.

Karato, S., Dupas-Bruzek, C., Rubie, D.C., 1998. Plastic deformation of silicate spinel under the transition-zone conditions of the Earth's mantle. Nature 395, 266–296.

Karato, S., Wang, Z., Liu, B., Fujino, K., 1995. Plastic deformation of garnets: systematics and implications for the rheology of the mantle transition zone. Earth Planet. Sci. Lett. 130, 13–30.

Karki, B.B., Stixrude, L., Wentzcovitch, R.M., 2001. High pressure elastic properties of major materials of earth's mantle from first principles. Rev. Geophys. 39, 507–534.

Kavner, A., Duffy, T.S., 2001. Strength and elasticity of ringwoodite at upper mantle pressures. Geophys. Res. Lett. 28, 2691–2694.

King, S.D., 1995. Models of mantle viscosity. In: Ahrens, T.J. (Ed.), AGU Handbook of Physical Constants. American Geophysical Unium, Washington, DC, pp. 227–236.

Kocks, U.F., 2000. Simulation of deformation texture development for cubic metals. In: Kocks, U.F., Tomé, C.N., Wenk, H.-R. (Eds.), Texture and Anisotropy: Preferred Orientations in Polycrystals and their Effect on Materials Properties. Cambridge University Press, Cambridge, pp. 390–419 (Chapter 9).

Lebensohn, R.A., Tomé, C.N., 1994. A self-consistent visco-plastic model: prediction of rolling textures of anisotropic polycrystals. Mater. Sci. Eng. A175, 71–82.

Lonardelli, I., Wenk, H.-R., Goodwin, M., Lutterotti, L., 2005. Rietveld texture analysis from synchrotron images of dinosaur tendon and salmon scale. J. Synchr. Res. 12, 354–360.

Lutterotti, L., Matthies, S., Wenk, H.-R., 1999. MAUD: a friendly Java program for materials analysis using diffraction. Int. U. Crystallogr. Comm. Powder Diffr. Newslett. 21, 14–15.

Matthies, S., Vinel, G.W., 1982. On the reproduction of the orientation distribution function of textured samples from reduced pole figures using the concept of conditional ghost correction. Phys. Status Solidi (b) 112, K111–K114.

Meng, Y., Fei, Y., Weidner, D.J., Gwanmesia, G.D., Hu, J., 1994. Hydrostatic compression of γ-Mg_2SiO_4 to mantle pressures and 700 K: thermal equation of state and related thermoelastic properties. Phys. Chem. Miner. 21, 407–412.

Merkel, S., Wenk, H.-R., Badro, J., Montagnac, J., Gillet, P., Mao, H.K., Hemley, R.J., 2003. Deformation of $(Mg_{0.9},Fe_{0.1})SiO_3$ perovskite aggregates up to 60 GPa. Earth Planet. Sci. Lett. 209, 351–360.

Merkel, S., Wenk, H.-R., Shu, S., Shen, G., Gillet, P., Mao, H.-K., Hemley, R.J., 2002. Deformation of polycrystalline MgO at pressures of the lower mantle. J. Geophys. Res. 107, 2271.

Miranda, C.R., Scandolo, S., 2005. Computational materials science meets geophysics: dislocations and slip planes of MgO. Comput. Phys. Commun. 169, 24–27.

Mitchell, T.E., 1999. Dislocations and mechanical properties of MgO–Al_2O_3 spinel single crystals. J. Am. Ceram. Soc. 82, 3305–3316.

Nishiyama, N., Wang, Y., Uchida, T., Rivers, M.L., Sutton, S.R., 2005. Pressure and strain dependence of the strength of sintered polycrystalline Mg_2SiO_4 ringwoodite. Geophys. Res. Lett. 32, L04307 (10.1029/2004GL022141).

Panasyuk, S.V., Hager, B.H., 1998. A model of transformational superplasticity in the upper mantle. Geophys. J. Int. 133, 741–755.

Rollett, A.D., Wright, S.I., 2000. Typical textures in metals. In: Kocks, U.F., Tomé, C.N., Wenk, H.-R. (Eds.), Texture and Anisotropy: Preferred Orientations in Polycrystals and their Effect on Materials Properties. Cambridge University Press, Cambridge, pp. 178–238 (Chapter 5).

Sasaki, S., Prewitt, C.T., Sato, Y., Ito, E., 1982. Single-crystal X-ray study of gamma-Mg_2SiO_4. J. Geophys. Res. 87, 7829–7832.

Singh, A.K., 1993. The lattice strains in a specimen (cubic system) compressed nonhydrostatically in an opposed anvil device. J. Appl. Phys. 73, 4278–4286.

Sinogeikin, S.V., Bass, J.D., 2001. Single-crystal elasticity of γ-$(Mg_{0.91}Fe_{0.09})_2SiO_4$ to high pressures and to high temperatures. Geophys. Res. Lett. 28, 4335–4338.

Stretton, I., Heidelbach, F., Mackwell, S., Langenhorst, F., 2001. Dislocation creep of magnesiowuestite ($Mg_{0.8}Fe_{0.2}O$). Earth Planet. Sci. Lett. 194, 229–240.

Thurel, E., Cordier, P., Frost, D.J., Karato, S., 2003. Plastic deformation od wadsleyite. Part II: high-pressure deformation in shear. Phys. Chem. Miner. 30, 267–270.

Tomé, C.N., Canova, G.R., 2000. Self-consistent modeling of heterogeneous plasticity. In: Kocks, U.F., Tomé, C.N., Wenk, H.-R. (Eds.), Texture and Anisotropy: Preferred Orientations in Polycrystals and their Effect on Materials Properties. Cambridge University Press, Cambridge, pp. 466–510 (Chapter 11).

Trampert, J., Van der Heijst, H.J., 2002. Global azimuthal anisotropy in the transition zone. Science 296, 1297–1299.

Uchida, T., Wang, Y., Rivers, M.L., Sutton, S.R., 2004. Yield strength and strain hardening of MgO up to 8 GPa measured in the deformation-DIA with monochromatic X-ray diffraction. Earth Planet. Sci. Lett. 226, 117–126.

Utsumi, W., Funamori, N., Yagi, T., Ito, E., Kikegawa, T., Shimomura, O., 1995. Thermal expansivity of $MgSiO_3$ perovskite under high pressures up to 20 GPa. Geophys. Res. Lett. 22, 1005–1008.

Wang, Y., Durham, W.B., Getting, I.C., Weidner, D.J., 2003. The deformation-DIA: a new apparatus for high temperature triaxial deformation to pressures up to 15 GPa. Rev. Sci. Instrum. 74, 3002–3011.

Weidner, D.J., Sawamoto, H., Sasaki, S., Kumazawa, M., 1984. Single-crystal elastic properties of the spinel phase of Mg_2SiO_4. J. Geophys. Res. 89, 7852–7860.

Wenk, H.-R., Lonardelli, I., Pehl, J., Devine, J., Prakapenka, V., Shen, G., Mao, H.-K., 2004. In situ observation of texture development in olivine, ringwoodite, magnesiowüstite and silicate perovskite at high pressure. Earth Planet. Sci. Lett. 226, 507–519.

Wenk, H.-R., Canova, G., Molinari, A., Mecking, H., 1989. Texture development in halite: comparison of Taylor model and self-consistent theory. Acta Metall. 37, 2017–2029.

Wenk, H.-R., Matthies, S., Donovan, J., Chateigner, D., 1998. BEARTEX: a Windows-based program system for quantitative texture analysis. J. Appl. Crystallogr. 31, 262–269.

Wookey, J., Kendall, J.M., Barruol, G., 2002. Mid-mantle deformation inferred from seismic anisotropy. Nature 415, 777–780.

Yamazaki, D., Karato, S., 2001a. Some mineral physics constraints on the rheology and geothermal structure of Earth's lower mantle. Am. Mineral. 86, 385–391.

Yamazaki, D., Karato, S., 2001b. High pressure rotational deformation apparatus to 15 GPa. Rev. Sci. Instrum. 72, 4207–4211.

Yamazaki, D., Karato, S., 2002. Shear deformation of (Mg,Fe)O: implications for seismic anisotropy in Earth's lower mantle. Phys. Earth Planet. Int. 131, 251–267.